Electrical conductivity of the thermal dusty plasma under the conditions of a hybrid plasma environment simulation facility

New Journal of Physics
The open access journal at the forefront of physics

Deutsche Physikalische Gesellschaft DPG
IOP Institute of Physics

Published in partnership with: Deutsche Physikalische Gesellschaft and the Institute of Physics

OPEN ACCESS

RECEIVED
23 January 2015

REVISED
11 April 2015

ACCEPTED FOR PUBLICATION
28 April 2015

PUBLISHED
27 May 2015

PAPER

Electrical conductivity of the thermal dusty plasma under the conditions of a hybrid plasma environment simulation facility

Dmitry I Zhukhovitskii[1], Oleg F Petrov[1,2,3], Truell W Hyde[3], Georg Herdrich[3,4], Rene Laufer[3,4], Michael Dropmann[3,4] and Lorin S Matthews[3]

[1] Joint Institute of High Temperatures, Russian Academy of Sciences, Izhorskaya 13, Bd. 2, 125412 Moscow, Russia
[2] Moscow Institute of Physics and Technology, 9 Institutskiy per., 141700 Dolgoprudny, Moscow Region, Russia
[3] Center for Astrophysics, Space Physics and Engineering Research (CASPER), Baylor University, One Bear Place #97310, Waco, TX 76798-7310, USA
[4] Institute of Space Systems (IRS), University of Stuttgart, Raumfahrtzentrum Baden-Wuerttemberg, Pfaffenwaldring 29, D-70569 Stuttgart, Germany

E-mail: dmr@ihed.ras.ru

Keywords: plasma, complex, thermal

Abstract

We discuss the inductively heated plasma generator (IPG) facility in application to the generation of the thermal dusty plasma formed by the positively charged dust particles and the electrons emitted by them. We develop a theoretical model for the calculation of plasma electrical conductivity under typical conditions of the IPG. We show that the electrical conductivity of dusty plasma is defined by collisions with the neutral gas molecules and by the electron number density. The latter is calculated in the approximations of an ideal and strongly coupled particle system and in the regime of weak and strong screening of the particle charge. The maximum attainable electron number density and corresponding maximum plasma electrical conductivity prove to be independent of the particle emissivity. Analysis of available experiments is performed, in particular, of our recent experiment with plasma formed by the combustion products of a propane–air mixture and the CeO_2 particles injected into it. A good correlation between the theory and experimental data points to the adequacy of our approach. Our main conclusion is that a level of the electrical conductivity due to the thermal ionization of the dust particles is sufficiently high to compete with that of the potassium-doped plasmas.

1. Introduction

Dust immersed in a weakly ionized plasma has long been recognized as a ubiquitous state of matter throughout the universe [1]. In space, dusty plasmas are found in protostellar clouds, planetary rings, cometary tails, and the interstellar medium [2–4]. On earth, the physics of dusty plasma is important in understanding the glow of a candle flame, lightning discharges in volcanic plumes [5], plasma processing of silicon wafers for computer chips [6], and the safety of tokamaks, such as ITER [7]. The basic physics and chemistry of dusty plasmas as well as their diagnostics and technological implications have been the subject of numerous papers (see for example [8] and the references therein) and possible applications such as nanostructured materials, plasma cleaning devices, adaptive electrodes, particle manipulation and modification are actively being investigated [9].

The dust particles in the plasma, ranging in size from tens of nanometers to hundreds of microns, become charged due to a variety of charging mechanisms. The amount of charging depends on the grain size, morphology, and composition, as well as the plasma environment [10–14]. In many environments, the equilibrium charge is mainly a result of the primary charging currents, in which electrons and ions within the plasma impinge upon and stick to the dust surface. However, there are some environments where secondary charging currents are the dominant charging mechanism: energy absorbed by the dust grain is gained by electrons, which are then emitted from the grain surface. These mechanisms include secondary electron

emission, photoemission, and thermionic emission [15–18]. It is possible in some cases for these emitted electrons to be major contributor to the electron density within the plasma, such as for UV-induced dusty plasmas [19, 20], or in flames, where the thermionic emission from carbonaceous soot elevates the electron density by several orders of magnitude [21, 22]. For a comprehensive discussion of these plasma types, see the review [23] and references therein. Recent studies based on the treatment of quantum states of the surplus electrons near the surface of charged particles make it possible to calculate such quantities as the electron sticking coefficient and desorption time, to account for the infrared extinction of dielectric particles etc [24–27].

The characteristics of such complex plasmas have implications for applications as disparate as understanding volcanic eruptions, the explosiveness of dust clouds and powders, communications, wildfires, rocket propulsion, and fusion energy. Lightning associated with volcanic plumes is a direct result of the electrification of the particulate matter within the plume. As these particles are transported over large distances, the electric potentials which develop lead to lightning discharges. The electrical activity of volcanic eruptions is a possible method to monitor volcanic activity, both here on earth and on exoplanets [28]. Many industries handle large amount of powders such as paint, chemical fertilizer, grain powder, starch, detergent. As airborne dust particles become charged, a spark introduced into the system can ignite an explosion [29]. Care must be taken during transport to mitigate the effects, which can lead to accidental dust explosions [30]. Wildfires are weakly ionized gas where the temperatures are great enough to cause thermal dissociation of the inorganic plant species drawn into the combustion zone. The conductor-to-ground short-circuiting caused by conductive wildfires is responsible for a number of the power outages in many countries [31]. The failure to maintain radio communication at HF to UHF during wildfire suppression is also a safety concern for fire fighters [32]. In a similar vein, spacecraft and vehicles traveling at hypersonic velocities within Earth's atmosphere become enveloped by a plasma layer which attenuates microwave and radio signals, leading to 'radio blackout' [33]. The ionized exhaust plumes also interfere with radio frequency transmission under certain conditions [34].

This effect can be put to good use, as the regression rates of solid rocket propellants have been measured using the attenuation of microwaves passing through flames [35]. However, 'background ionization' of particles must be taken into account quantitatively in order to properly interpret the data [21], and a more sensitive method for obtaining the concentration of electrons in luminous flames is to determine the conductivity of the flame [22]. Such data can also be used in the design of divertors [36, 37]. Note that carbon particles in the plasma environment which are to be encountered in these devices are similar to the carbon particles in the complex plasma of flames investigated in the pioneer works in the field of thermal dusty plasma [21, 22, 38, 39].

The development of the inductively heated plasma generator (IPG) enables the electrode-less generation of high enthalpy plasmas, such as those found in the divertor region of fusion experiments or plasma wind tunnels, for the simulation of atmospheric entry in the development, investigation, and qualification of heat shield materials [40].

The objective of this paper is to develop a theoretical method for the estimation of the electrical conductivity of the thermal plasma formed by the dust particles and the electrons emitted by them in the state of thermal ionization equilibrium under typical conditions of the IPG6-B at Baylor University. We will completely ignore ionization of impurities entering into the carrier gas from the particle material, the effect of these impurities on the work function of the particle material, and carrier gas ionization. The magnitude of the electrical conductivity in an equilibrium plasma is determined by two factors, namely, the electron number density and the frequency of collisions with the molecules of the carrier gas and the dust particles. As shown in what follows, the contribution to the total collision frequency from collisions with the dust particles is inversely proportional to the particle radius at a constant mass fraction of particles in the plasma. However, even for the smallest particle size, this contribution does not exceed the contribution due to collisions with molecules of the carrier gas, the frequency of which can be regarded as known (it is determined by the composition of the plasma). Therefore, the problem of calculating the plasma conductivity is reduced to the problem of calculating the number density of electrons in the plasma. For different temperatures, pressures, and particle composition, various plasma states from an ideal to strongly coupled one are realized. However, regardless of the state, an estimate for the maximum particle charge can be written and, therefore, in view of the condition of quasineutrality, for the maximum electron number density as well. It turns out that this number density increases dramatically with decreasing particle radius. To reach the maximum conductivity it makes sense to use the smallest possible particle radius, which results from the volume condensation of a material with a small work function. We analyze available data on the electrical conductivity of the thermal dusty plasma. The correspondence between our theory and experiment demonstrates the relevance of our approach. This makes it possible to calculate some reference values of the electrical conductivity typical for the conditions of the hybrid IPG facility at Baylor University.

The paper is organized as follows. In section 2, the IPG is discussed in detail. In sections 3 and 4, the electron mean free path and number density are calculated allowing the determination of the plasma electrical conductivity. In section 5, we demonstrate a good correlation between our calculations and available

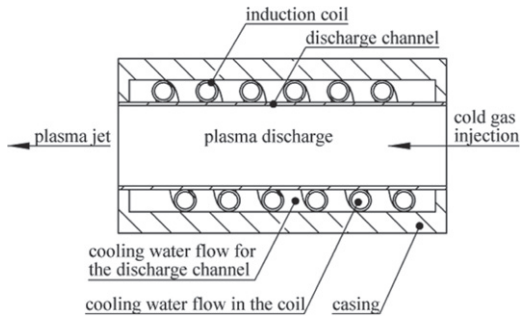

Figure 1. Working principle of an inductively heated plasma generator.

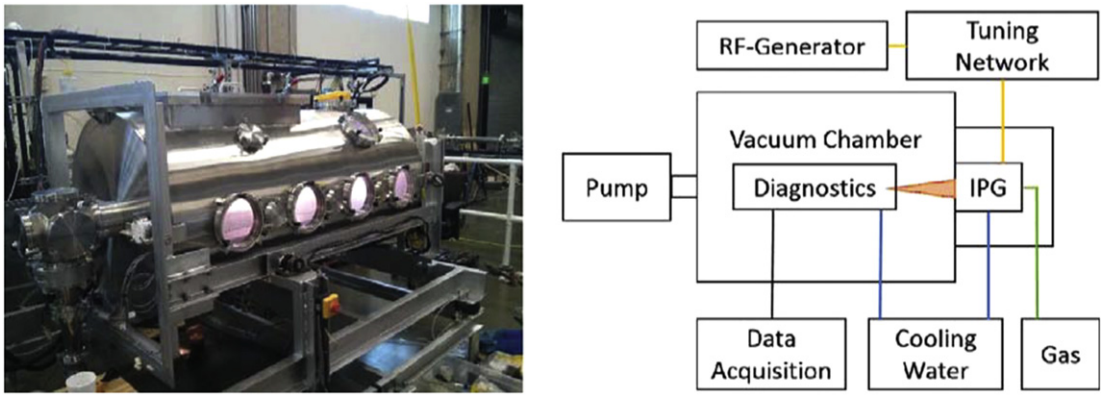

Figure 2. Left: IPG6-B test facility in operation with working gas helium. Right: block diagram of the test facility.

experimental data. In section 5.1, emphasis is made on a recent experiment with the thermal dusty plasma of combustion products of the propane–air mixture [41–43]. In section 5.2, we calculate the plasma electrical conductivity to be expected in experiments with the IPG6-B. The results of this study are summarized in section 6.

2. The IPG facility

IPGs use the transformer principle to create a plasma. An RF (radio frequency) current is fed into a coil inducing a strong electric field in the plasma which acts like the secondary coil of a transformer, with plasma heating then occurring due to the resulting electric current. A rough scheme of the IPG6-B working principle is shown in figure 1 (for details, see [40, 44]). Cold gas is injected into one side of the plasma generator. By adding an azimuthal component to the gas flow, stabilization of the plasma can be achieved. After injection, the gas enters the quartz tube discharge channel, which can withstand both high temperatures and reactive gases. The discharge channel is surrounded by a water jacket to facilitate cooling. Further it is surrounded by the induction coil, which heats the plasma. The IPG6 test facilities at the University of Stuttgart (IPG6-S) and at Baylor University (IPG6-B; figure 2) are small scale versions of the IPGs IPG3, 4, and 5 at IRS [45]. The general setup for both facilities is similar. The IPG6-B test facility and its schematic setup are shown in figure 2. Important operating parameters are listed in table 1.

3. The mean free path of electrons in a dusty plasma

The electron mean free path is determined by the number of collisions between the dust particles and carrier gas molecules. The mean free path of collisions with the particles can be estimated using the formula $\lambda_p = 1/n_p\sigma_p$ where n_p is the number density of the dust particles, and σ_p is the electron-particle scattering cross section. Regardless of whether the plasma formed by the dust particles and the electrons emitted by them is strongly coupled in the parameter of the particle–particle interaction, the plasma is quasi-homogeneous in the spatial distribution of the electron number density [46]. This means that the electrostatic potential of a charged particle

Table 1. Important operating parameters of the IPG6-B test facility.

Parameter	Value	Comment
Operating frequency	13.56 MHz	—
Vacuum system	160 $m^3 h^{-1}$	—
Maximum electric power	15 kW	A maximum of 5 kW has been tested.
Volume flow rate	0.35–10 slm	A wider range is possible.
Operating pressure	>20 Pa	Lower limit due to vacuum pump. Upper limit not tested yet. Maximum used pressure is 400 Pa.
Gases	He, Ar, O_2, Air	The IPG can theoretically work with most gases including oxidizing gases.
Specific enthalpy	He: several 100 MJ kg^{-1} Air: several 10 MJ kg^{-1}	The specific enthalpy depends strongly on the working gas, the respective efficiency and mass flow rate.
Flow velocity	Ma < 0.3	A nozzle will allow supersonic flows in future.

is screened at a distance of the order $\bar{r}/2$ (see equation (8)), where $\bar{r} = (3/4\pi n_p)^{1/3}$ is the radius of the cell in a cell model of the plasma (i.e., $\bar{r}$ is of the order of the average distance between the particles in the plasma). Obviously, σ_p cannot exceed $\pi\bar{r}^2/4$. Therefore, one can use $\sigma_p = \pi\bar{r}^2/4$ as a lower bound estimate for λ_p. We introduce the quantity $\kappa = n_c/n_g$, the mole fraction of particulate dust matter in the combustion products, where $n_c = (4\pi/3)R^3 n_p n_\ell$ is the number of molecules in the condensed phase per unit volume of the plasma, R is the dust particle radius, n_ℓ is the number density of molecules in the condensed phase, and n_g is the number density of molecules of the carrier gas (i. e., of the combustion products). In this case, the lower bound estimate for λ_p,

$$\lambda_p \geqslant \frac{16}{3}R\left(\frac{n_\ell}{\kappa n_g}\right)^{1/3}, \tag{1}$$

is directly proportional to the particle radius.

For collisions with the carrier gas molecules, we have the mean free path

$$\lambda_g = \frac{1}{n_g k^2\, T^2}\int_0^\infty \frac{\varepsilon e^{-\varepsilon/kT}}{\sigma_g(\varepsilon)}\,\mathrm{d}\varepsilon, \tag{2}$$

where $\sigma_g(\varepsilon)$ is the transport cross section for electron scattering by molecules of the carrier gas . Consider as representative example the combustion of hydrocarbon fuels with a temperature $T = 2500$ K ($kT = 0.215$ eV) at atmospheric pressure $p_g = n_g kT = 1$ atm, where k is the Boltzmann constant, and $n_g = 3\times 10^{18}$ cm^2. We assume that the major components of the combustion products are molecules of nitrogen (78%), carbon dioxide (12%) and oxygen (10%) (excess air). The transport scattering cross sections for these molecules are given in [47]. Under these conditions, $\sigma_g \sim 10^{-15}$ cm^2, and we obtain from equation (2), $\lambda_g = 3\times 10^{-4}$ cm. To establish a lower bound of λ_p, we choose the smallest possible particle size $R = 10^{-6}$ cm and the greatest part of the mole fraction attainable for this size $\kappa = 0.02$. Then we obtain from equation (1) $\lambda_p \geqslant 4.2\times 10^{-4}$ cm. Thus, for combustion products $\lambda_p > \lambda_g$, regardless of the dust particle size and number density. This condition means that when calculating the plasma conductivity one can always neglect collisions between particles and calculate the conductivity using the formula [48]

$$\begin{aligned}\sigma &= \frac{10^{11}}{c^2}\frac{4\lambda_g n_{e0}e^2}{3\sqrt{2\pi m_e kT}} = \frac{10^{11}}{c^2}\frac{4n_{e0}e^2}{3n_g k^2\, T^2\sqrt{2\pi m_e kT}}\int_0^\infty \frac{\varepsilon e^{-\varepsilon/kT}}{\sigma_g(\varepsilon)}\,\mathrm{d}\varepsilon \\ &= \frac{10^{11}}{c^2}\frac{4n_{e0}e^2}{3n_g\bar{\sigma}_g\sqrt{2\pi m_e kT}}, \quad \frac{1}{\bar{\sigma}_g} = \frac{1}{kT}\int_0^\infty \frac{\varepsilon e^{-\varepsilon/kT}}{\sigma_g(\varepsilon)}\,\mathrm{d}\varepsilon,\end{aligned} \tag{3}$$

where σ is the conductivity in S m^{-1} and other quantities are measured in CGS units, c is the speed of light, e is the elementary charge, m_e is the mass of the electron, and n_{e0} is the electron number density.

4. The electron number density in the equilibrium dusty plasma

Consider a complex (dusty) plasma formed by the positively charged dust particles and the electrons emitted by them and assume the plasma to be in a state of thermal ionization equilibrium. Assuming that the fluctuations of the particle charge are small (which is true if the charges are sufficiently great), we denote by Z the charge (in units of e) of a particle with the radius R. At the ionization equilibrium, the local number density of electrons $n_e(r)$ at the distance r from the center of a particle is defined by the Boltzmann distribution

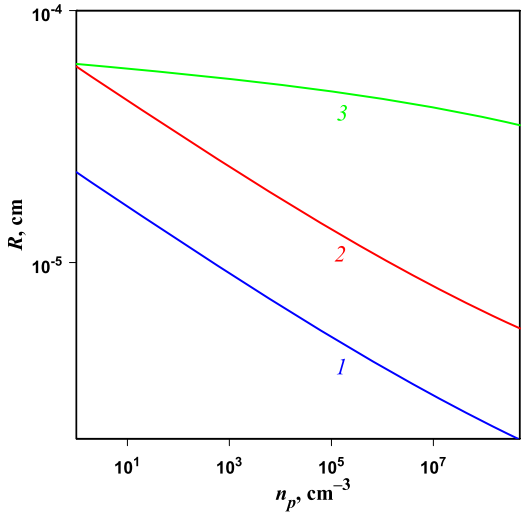

Figure 3. Regions of dusty plasma states for $T = 2500$ K and $W = 2.75$ eV. Boundaries of the ideal and strongly coupled plasmas are indicated by curves 1 and 2, respectively; curve 3 indicates the boundary between the regimes of weak and strong screening.

$$n_e(r) = n_{e0}\mathrm{e}^{\Phi(r)}, \tag{4}$$

where $\Phi(r) = e\varphi(r)/kT$ and $\varphi(r)$ is the electrostatic potential of the particle charge at the distance r from the center of a particle.

First we consider the case of a weak interaction between the particles, for which the interparticle interaction parameter is small: $\gamma_{pp} = Z^2e^2/\bar{r}kT \ll 1$. Since a particle bears typically a great charge ($Z \gg 1$), the parameters of interaction between the particles and electrons $\gamma_{pe} = Ze^2/\bar{r}kT$ and $\gamma_{ee} = Z^{1/3}e^2/\bar{r}kT$ are particularly small. As can be seen in figure 3, screening of the particle charge is negligibly small if $\gamma_{pp} \ll 1$ (see the discussion below). Then we can neglect the contribution of inhomogeneity of the electron distribution in the vicinity of the particles to the quasineutrality condition and write it as $n_{e0} = Zn_p$ [46, 49]. At the particle surface, we have from equation (4) $\Phi(R) = L_1$, where $L_1 = \ln(n_{es}/n_{e0})$,

$$n_{es} = 2\left(\frac{m_ekT}{2\pi\hbar^2}\right)^{3/2}\exp\left(-\frac{W}{kT}\right) \tag{5}$$

is the number density of the thermally emitted electrons near the surface of a particle [39], and W is the work function of its material. Here, we suggest that W is independent of R. Since $\varphi(R) = Ze/R$, we obtain the particle charge and the electron number density [38, 39, 46, 49]

$$Z = \frac{RkT}{e^2}L_1, \quad n_{e0} = \frac{RkTn_p}{e^2}L_1. \tag{6}$$

Consider now an opposite case ($\gamma_{pp} \gg 1$), in which, at least, a short-range order in the particle spatial position must take place. Then the plasma is divided in cells with the radius $\bar{r}$ similar to the Wigner–Seitz cells. The combination of equation (4) with the Poisson equation inside a cell $\Delta\Phi = (4\pi e^2/kT)n_e(r)$ leads to the Poisson–Boltzmann equation

$$\frac{\mathrm{d}^2\Phi}{\mathrm{d}r^2} + \frac{2}{r}\frac{\mathrm{d}\Phi}{\mathrm{d}r} = \lambda_D^{-2}\mathrm{e}^{\Phi}, \tag{7}$$

where $\lambda_D = \sqrt{kT/4\pi n_{e0}e^2}$ is the Debye length, with the boundary conditions $\Phi'(R) = -Ze^2/kTR^2$ and $\Phi'(\bar{r}) = 0$ (the latter condition is due to the cell electrical neutrality).

Here, we will distinguish between the cases of weak and strong screening of the particle charge. As is seen from (4), the electrons form a layer in the vicinity of the particle surface. If the absolute value of this charge is much less than the particle charge, the weak screening regime is realized. In addition, if $R \ll \bar{r}$ then in the most part of the cell (sufficiently far from the particle), the distribution of electrons is almost uniform, i.e., $\Phi(r) \ll 1$, and the solution of equation (7) has the form

$$\Phi(r) = \frac{\bar{r}^2}{3\lambda_D^2}\left[\frac{\bar{r}}{r} - \frac{3}{2} + \frac{1}{2}\left(\frac{r}{\bar{r}}\right)^2\right]. \tag{8}$$

In the opposite case, a layer of electrons in the neighborhood of a particle screens strongly its charge. One can assume that this occurs in a thin layer, in which the problem is one-dimensional and the condition $(2\lambda^2/r)|\mathrm{d}\Phi/\mathrm{d}r| \ll 1$, where $\lambda = \sqrt{kT/4\pi n_e(r)e^2}$ is the local Debye length, is satisfied. Hence, the maximum charge that is weakly screened or the minimum charge that is strongly screened Z^* is defined by the condition

$$\frac{2\lambda^2}{R}\left|\frac{\mathrm{d}\Phi}{\mathrm{d}r}\right|_{r=R} = 1. \tag{9}$$

In the regime of the weak screening, the condition of cell neutrality can be written as $n_{e0} \simeq Zn_p$. Then it follows from (8) that near the particle surface, $\Phi(r) \simeq RL_1/r$. We substitute this in (9) to derive $L_1 = L_2$ and $Z^\star = RkTL_2/e^2$, where the quantity

$$L_2 = -\ln\left(2\pi n_p R^3\right) \tag{10}$$

is independent of n_{es}, i.e., of the emissivity of the particle material [46, 49].

In the regime of the strong screening, we have $R^2/\lambda_S^2 \gg 2L_1$, where $\lambda_S = \sqrt{kT/4\pi n_{es}e^2}$ is the surface Debye length. In this case, we assume that near the particle surface, $\Phi(r)$ decreases with the increase of r until the condition (9) is satisfied at some point $r = R_1$. If $(R_1 - R)/R \ll 1$ then the total charge inside the sphere with the radius R_1, which can be termed the effective charge, is $Z^\star$. In the most part of the cell ($r > R_1$), the weak screening regime still takes place for the effective charge, and the electron number density is defined by the ratio

$$n_{e0} = \frac{RkTn_pL_2}{e^2}. \tag{11}$$

Note that (11) is independent of the particle emissivity. The above-discussed model reproduces to a reasonable precision the results of numerical solution of the Poisson–Boltzmann equation (7) [50].

We can summarize the obtained results as follows. Regardless of the value of the parameter γ_p, the particle charge is defined by the expression

$$Z = \frac{RkT}{e^2}L, \tag{12}$$

and the electron number density is

$$n_{e0} = \frac{n_pRkT}{e^2}L = \frac{3}{4\pi}\frac{\kappa p_g}{R^2e^2n_\ell}L, \tag{13}$$

where

$$L = \min(L_1, L_2), \quad L_1 = \ln(n_{es}/n_{e0}),$$
$$L_2 = -\ln\left(2\pi n_pR^3\right) = \ln\left(\frac{2n_\ell}{3\kappa n_g}\right). \tag{14}$$

For small n_{es}, $n_e \approx n_{es}$, and by virtue of the quasineutrality condition, the particle charge is positive, $Z > 0$ and $n_e < n_{es}$. Thus, $L = L_1$. Then, with an increase of n_{es} (due to an increase in temperature or decrease in the work function), L_1 and L increase until they reach L_2. After that, L does not change. Consequently, an estimate for the maximum number density of electrons in the plasma $n_{\max}$, which is attained at sufficiently low W and coincides with that at $W = 0$, is given by the expression

$$n_{\max} = \frac{3}{4\pi}\frac{\kappa p_g}{R^2e^2n_\ell}\ln\left(\frac{2n_\ell}{3\kappa n_g}\right). \tag{15}$$

The difference between the actual and the maximum electron number density is given by the ratio $n_e/n_{\max} = L/L_2$.

For the above conditions typical for combustion products of hydrocarbon fuels, $L_2 = \ln(2n_\ell/3\kappa n_g) = 12.7$. When $L = L_1 < L_2$, the charges on the particles are weakly screened by the electrons near the surface, while at $L = L_2 < L_1$ ($n_e = n_{\max}$), they are strongly screened. In the first case, (12) defines a real dust particle charge, while in the second case, it defines an effective one, which is equal to the difference between the actual charge of the particle and the charge of the screening layer of electrons near the surface.

Figure 3 shows the state diagram for the dusty plasma with respect to the parameter of dust interparticle interaction. The ideal plasma region is located below curve 1 ($\gamma_p = 1$) and a strongly nonideal plasma region situated above curve 2. Curve 2 was calculated for $\gamma_p = 6.4$, which corresponds to the emergence of a short-range order in the model of one-component plasma of electrons and ions [51]. In the region above curve 3 ($L_1 = L_2$) particles are in the strong screening regime, while below curve 3, they are in the weak screening regime.

Table 2. Parameters of the work function of dust particle material [52].

	CaO	BaO	CeO_2
A, eV	1.32	1.40	2.75
B, 10^{-4} eV K^{-1}	4.5	7.0	0.0

Table 3. Electron work function of CaO.

T, K	W, eV, processing the data [53]	W, eV, extrapolation of the data [54]
2200	3.35	3.29
2400	3.43	3.42
2530	3.79	3.51

As can be seen in the figure, at $R \gtrsim 10^{-4}$ cm, the particle charge is strongly screened and the particles typically form a strongly coupled system, while at $R \lesssim 10^{-5}$ cm, the particle charge is weakly screened and the particle system can be strongly coupled only at high particle number densities. At $R \lesssim 10^{-6}$ cm, the particle charge is always weakly screened and the particle system is almost ideal.

From formulas (3) and (15), it follows that the theoretical limit for experimentally achievable conductivity of the plasma formed by the dust particles and the electrons emitted by them is given by

$$\sigma_{\max} = \frac{10^{11}}{c^2}\frac{\kappa}{R^2 n_\ell \bar{\sigma}_g}\sqrt{\frac{kT}{2\pi^3 m_e}}\ln\left(\frac{2n_\ell}{3\kappa n_g}\right). \tag{16}$$

It is worth mentioning that the electrical conductivity (16) is weakly dependent on the temperature, since the ratio $\sqrt{T}\,\bar{\sigma}_g(T)$ is approximately proportional to T, but it is sensitive to the average size of the particles being inversely proportional to its square. Therefore, to achieve a high electrical conductivity it makes sense to use only smaller particles. For conditions of the experiments [41–43] at $R = 10^{-6}$ cm, when $T = 2500$ K, $\kappa = 0.02$, $n_\ell = 3.62 \times 10^{22}$ cm^{-3}, and $\bar{\sigma}_g = 10^{-15}$ cm^2, we have $n_{\max} = 7.4 \times 10^{12}$ cm^{-3}, $Z = 19$, and $\sigma_{\max} = 2$ S m^{-1}.

5. Comparison between the calculation results and experimental data

5.1. Early experiments

Calculation of the electric conductivity of a thermal dusty plasma with the particles of CaO, BaO, and CeO_2 was carried out using equations (3), (13), and (14) for different temperatures and buffer gases. In so doing, we took into account the dependence of the work function of the particles on the temperature, which significantly affects the emission properties of their material. The work function of the particle material was approximated by the expression $W = A + BT$ with the constants A and B shown in table 2.

In [53], the conductivity of methane–air (oxygen–methane) combustion products mixed with fine powders of CaO and BaO was measured. The temperature was varied in the range from 2200 to 2530 K, and the powder flow rate, from 0.2 to 18% of the mass flow rate of combustion products. The measured conductivity varied from 0.01 to ca. 0.3 S m^{-1}, and the data scatter was considerable. A considerable uncertainty in the particle radius R is characteristic of this experiment. We will assume that according to the state classification of section 6, the dust particles are weakly screened, and, therefore, the electron number density is defined by equation (12) with $L = L_1$. Assuming in addition that the ratio of the mass flow rate of the powder to that of the combustion products is $\beta = \rho_\ell \kappa / M_g n_\ell$, where ρ_ℓ is the specific weight of the particle material and M_g is the average mass of the combustion products molecule, we rewrite equation (3) in the form

$$\ln\beta = \ln\sigma - \ln\left(\ln\frac{10^{11}}{c^2}\frac{4e^2 n_{es}}{3n_g\bar{\sigma}_g\sqrt{2\pi m_e kT}} - \ln\sigma\right) - \ln\left(\frac{10^{11}}{c^2}\frac{M_g}{\pi R^2\rho_\ell\bar{\sigma}_g}\sqrt{\frac{kT}{2\pi m_e}}\right), \tag{17}$$

where n_{es} (5) is a function of W. Thus, the dependence $\ln\beta(\ln\sigma)$ is almost linear. We fitted the experimental data [53] by variation of W and R in (17). This allowed us to determine these quantities. As a result, for CaO, we obtained a good agreement between the values of W obtained by processing the experimental data and extrapolation to the high-temperature region of the results of the work function measurement for CaO [54] (see

table 3). Note, however, that at $T > 2000$ K, there is a considerable discrepancy between the extrapolation of the data [54] and [52]. The values of R also derived from the processing of the experiment, are in qualitative agreement with the estimate [53]: $(1 \pm 0.5) \times 10^{-5}$ cm.

Comparison of the theory and experiment for BaO particles for the considered experiment is impossible because in this temperature range, a significant portion of barium is in the gas phase (melting point of BaO is 2196 K), and it can be shown that the ionization of BaO molecules is comparable with the corresponding ionization of the dust particles.

In the experiment [55], the electrical conductivity of the plasma with the particles of BaO in argon at $T = 1600$ K was measured. The mass flow rate of BaO particles with the radius $R = 3 \times 10^{-5}$ cm was $\beta = 0.2$ of the argon mass flow rate ($\kappa = 0.05$); the measured conductivity was 0.1 S m^{-1}. Under these conditions, the temperature is low, so the ionization of barium compounds is negligible. Calculation of the effective cross section for electron scattering yields $\bar{\sigma}_g = 2.49 \times 10^{-17}$ cm^2, and from formulas (3), (13), and (14), we obtain a theoretical estimate for the electrical conductivity $\sigma = 0.12$ S m^{-1}, which is in a good agreement with experiment.

5.2. Recent experimental data and prospects

Consider the experiment performed at the Joint Institute for High Temperatures, Russian Academy of Sciences, where the particles of CeO_2 were injected into the plasma of combustion products of the propane–air mixture. The experimental facility includes a plasma generator and the diagnostic means for determining the parameters of the particles and gas [56]. The main part of the plasma source consists of a two-flame propane–air Meeker burner with inner and outer flames. The laminar diffusion flame design was used to support a premixed propane–air flat flame and provide a uniform exit profile of the plasma parameters (temperature, velocity, and electron and ion densities). To shield the flame from entrained room air, a central region, 25 mm in diameter, of the burner surface was surrounded by a shroud of combustion gases flowing through an annular area with inner and outer diameters of 25 and 50 mm, respectively. During operation, the velocity V_g of the plasma stream was varied over $2 \div 3$ m s^{-1} and the electron number density in the flame, over $10^9 \div 10^{11}$ cm^{-3}. The temperatures of the electrons and ions were equal and were varied over the range $T_i = T_e = T_g = 1700 \div 2200$ K, where T_g is the gas temperature. The spectroradiometric measurements of the temperature of the particles T_p [57] showed that it was close to the gas temperature ($T_p \approx T_g$). The combustion products were at atmospheric pressure.

We studied thermal plasma with two types of chemically inert particles, Al_2O_3 and CeO_2. The dust particles were slightly impure and contained sodium and potassium. As a result, the spectra measurements revealed that a plasma spray of particles contains sodium and potassium atoms, which have a low ionization potential. Typical plasma spectra include continuous dust radiation and K spectral lines (see figure 2 of [58]).

In our experiments we use the plasma of combustion products of the propane–air mixture in stoichiometry, so we may expect that the combustion products will not contain soot (carbon) dust. Thus, the main components of the plasma in one case were charged CeO_2 particles, electrons, and singly charged Na^+ ions, and, in the other, charged Al_2O_3 particles, electrons, and Na^+ and K^+ ions. The measurements of the gas temperature and the number densities of sodium and potassium atoms were carried out with the aid of the generalized line reversion and full-absorption techniques, correspondingly (the errors were less than 1% and 30%, respectively) [56]. The local density n_i of positive ions was determined by an electrical probe method [59]. Under typical experimental conditions, the diagnostic measurements showed that the ion number density ($n_i \sim 10^9$ cm^{-3}) appeared to be almost an order of magnitude lower than the electron number density ($n_e \sim 10^{10}$ cm^{-3}). The estimate based on the experimentally determined Na and K atom number densities and the Saha equation results in the electron number density, which is much lower than the measured one. Hence, it follows from the plasma quasineutrality condition that the contribution from the ionization of the Na and K admixtures to the total electron number density (and, respectively, to the electrical conductivity of the complex plasma) is negligibly small as compared to that from the electrons emitted by the dust particles. In order to study Coulomb ordered structures in the plasma, it is necessary to have data on the charge of the particles, as well as on the basic plasma parameters. An important feature of this plasma device is that it provides a dusty plasma of large enough dimensions (plasma column of 25 mm diameter and 70 mm long) so that a variety of plasma experiments may be conducted. As a result, various parameters of the gas and macroscopic particles were determined, such as the electron and alkali ion densities, the gas temperature, and the size and density of the macroparticles.

The plasma was diagnosed by probe and optical techniques. The arrangement of the probe measurements is shown in figure 4. The density n_i of the positive alkali metal ions was measured with an electrical probe [41, 42]. The random error in n_i results in an uncertainty of 20%. The local electron number density n_e was determined by a method based on measuring the current I and longitudinal electric field E in the plasma [59]. An electrode at constant voltage relative to the burner was placed in the plasma flow to determine the current I. Two probes were introduced into the plasma to determine the tangential component E of the electric field. The electrical

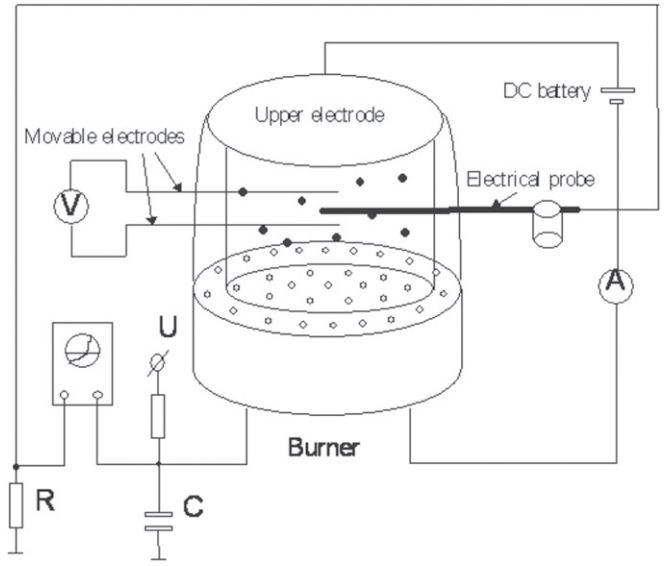

Figure 4. The arrangement of the probe measurements. It includes (1) the electrical probe to measure the number density of the positive alkali metal ions n_i and (2) the upper electrode at constant voltage relative to the burner and two movable probes to determine the current I and the tangential component E of the electric field, respectively (for the electron number density characterization). Open dots are holes in the top of the burner and filled dots are the dust particles.

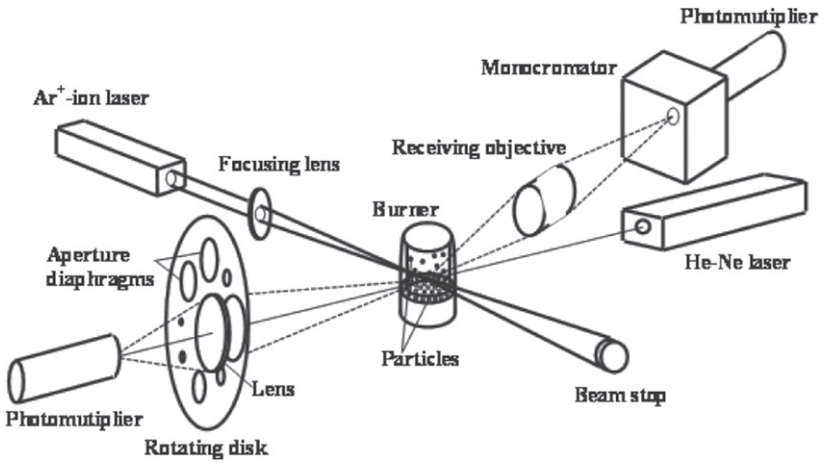

Figure 5. The setup for the optical measurements of the sizes, density, and spatial structures of the macroparticles.

conductivity of the plasma $\sigma = n_e e\mu_e$ was determined on the basis of Ohm's law $j = \sigma E$ (j is the current density and μ_e is the mobility of the electrons). The electron number density was found from known μ_e. The uncertainty in the electron number density n_e did not exceed 30%. The original laser method is used for characterization of the mean diameter and density of dust particles in the plasma flow. The method is based on the measurements of transmittance (extinction of a light beam passing through a dispersed medium) at small scattering angles. This technique is intended for determining the characteristics of particles with sizes of $0.5 \div 15$ μm. The setup for measuring the extinction of optical radiation includes a rotating disk with aperture stops of various diameters located in front of a photodetector (figure 5). A He–Ne laser ($\lambda = 0.633$ μm) is used as the light source. For an error in the measurement of the extinction of about 2%, the errors in recovering the particle sizes and density were about 3% and 10%, respectively. The ordered structures were analyzed using the binary correlation function [41] obtained with a laser time-of-flight counter (figure 5). The measurement volume is formed by focusing the beam of an Ar^+ laser (wavelength $\lambda = 0.488$ μm) onto the axial region of the plasma stream. Radiation scattered by individual particles at the angle of 90° when they cross the waist of the laser beam is collected by a lens and directed onto the 15 μm-wide monochromator entrance slit. The diameter of the measurement volume was less than 10 μm. The resulting pulsed signals were then processed to calculate the pair correlation function $g(r)$, which characterizes the probability of finding a particle at a distance $r = V_p t$ from a given particle. Here, t is the time and V_p is the average particle velocity ($V_p \approx V_g$ for micron-sized particles

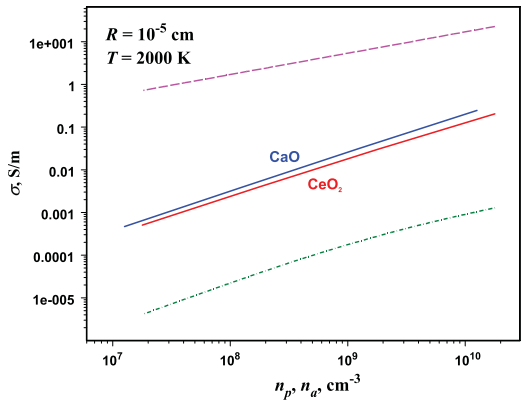

Figure 6. Conductivity of the combustion products plasma with the dust particles of the radius 10^{-5} cm (blue solid line denotes the CaO particles and red solid line, the CeO_2 particles) and of the combustion products plasma doped with potassium seed: dashed line corresponds to equal mass fractions of the particles and the seed and dashed–dotted lines, to the condition $n_a = n_p$.

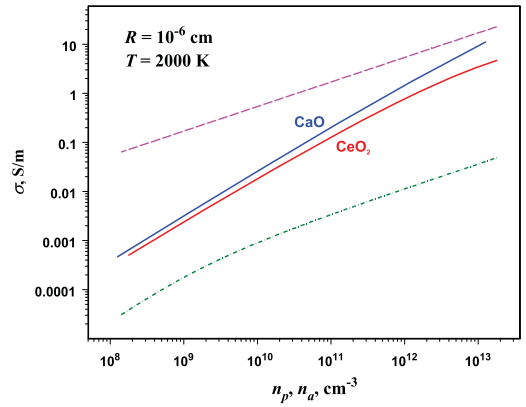

Figure 7. Same as in figure 6 for the particles of the radius 10^{-6} cm.

[41, 42]). An analysis of $g(r)$ makes it possible to describe the spatial structure and interparticle correlations of the particles.

If we estimate the average radius of CeO_2 particles as 8×10^{-5} cm and take into account that their number density ranges from 0.2×10^7 to 5.0×10^7 cm^{-3} then at $T = 1700 \div 2200$ K, the particle charge is weakly screened according to the condition $L_1 < L_2$ (equation (14). Hence the electron number density estimated by formulas (13) and (14) which yield $n_e \simeq (2.2 \div 4.2) \times 10^{10}$ cm^{-3}. This result agrees well with the experimentally determined value of $(2.5 \div 7.2) \times 10^{10}$ cm^{-3}. Based on the thermodynamic data [60] it can be shown that the equilibrium ionization of CeO_2 molecules in the gas phase is negligibly small as compared with the ionization of the dust particles. This means that the main contribution to the electron number density is that from the electrons produced by thermonic emission from the macroparticles. According to the state classification of section 4, the dust particles form a strongly coupled system, i. e., the particle positions must be noticeably correlated. This also agrees with the correlations registered in the above-discussed experiment.

In figures 6 and 7, the conductivity of the plasma combustion products of hydrocarbon fuels with CeO_2 and CaO particles is compared with the electrical conductivity of the combustion products when doped with potassium at $T = 2000$ K. Similar plasma parameters are expected for the IPG facility discussed in section 2. The component composition of the combustion products was calculated using [60]. In these figures, the lower limit of the range of n_p is defined by the minimum electrical conductivity that can be reliably measured in experiment. An upper limit corresponds to the mole fraction of particulate matter in the combustion products $\kappa = 0.52$, which can be considered the maximum attainable in the experiment. The seed ionization was calculated by the Saha equation. It is seen that for the particles with the radius 10^{-6} cm at sufficiently large n_p, the electrical conductivity of dusty plasma has the same order of magnitude as the potassium-doped combustion products even for equal mass fraction of particles and seed in the combustion products, and when $n_a = n_p$, where n_a is the

number density of seed atoms, the electrical conductivity of dusty plasma exceeds that of the combustion products significantly.

6. Conclusion

In this paper, we have discussed the IPG facility and developed a theoretical method for the estimation of the electrical conductivity of the thermal plasma formed by the dust particles and the electrons emitted by them under typical conditions of the IPG facility. To this end, we first find that under these conditions, the electron mean free path is defined by collisions with the neutral gas molecules rather than with charged particles. Then we calculated the equilibrium electron number density and demonstrated that for any given dust particle radius there existed an upper bound for the electron number density, which is reached when the electron work function from the particle material is sufficiently low, and the particle charge is strongly screened by the electron gas in the vicinity of the particle surface. Correspondingly, there is a similar upper bound for the electrical conductivity of the plasma. In the vicinity of this upper bound, the conductivity is independent of the electron work function and depends weakly on the temperature.

To verify our calculation formulas, we analyzed available experimental data on the conductivity of thermal dusty plasma and discussed in detail a recent experiment, where particles of CeO_2 were injected into a plasma consisting of the combustion products of a propane–air mixture. A good agreement between the theory and experiment testifies to the relevance of our theoretical approach. Employing this approach we make the estimates for future experiments on the IPG facility and show that the level of attainable electrical conductivity is competitive with that of the plasmas doped with potassium.

Although our theory is in satisfactory agreement with available experimental data, these data are currently too few in number to draw definitive conclusions. Calculation of the conductivity of a dusty plasma is also complicated by a considerable uncertainty in the work function of the particle material W, the particle radius R, and the effective transport cross section for electron scattering by the carrier gas molecules $\bar{\sigma}_g$ involved in the calculation formulas. Large scatter in the values of W for the same substance at the same temperature (about 1 eV) available in the literature has already been discussed above. In particular, this scatter can be due to the admixtures adsorbed on the particle surface. Values of R, which are not always precisely known even for the powder used in the plasma of combustion products, can vary significantly due to cracking of the particles during thermal shock at the moment of their introduction into the plasma and due to partial evaporation of the particle material and its subsequent nucleation to form a new fine fraction. Calculation of $\bar{\sigma}_g$ in the combustion products requires a detailed calculation of their component composition, which is a separate problem.

Despite the difficulties of theory and experiment, we can conclude that the maximum electrical conductivity, which is proportional to R^{-2} (see (16)), can only be achieved in a plasma containing extremely small particles. As such, it may make sense to create experimental conditions suitable for initial particle evaporation and subsequent nucleation of the substance. Note that in some technologies, the effect of enhancing the electrical conductivity due to the particles may be undesirable. It is known that during the process of nucleation in the combustion products, microdroplets with a characteristic size $R \sim 10^{-6}$ cm are formed [61]. Their ionization can lead to large values of σ. Apparently, BaO particles should be regarded as most promising for such purposes. For more conventional experiments, where the size range of particles to be injected into the plasma is assumed to be controlled, it makes sense to use LaB_6 .

The model introduced in this paper may be a simplified approach due to its equilibrium assumptions. However, for equilibrium conditions it has to be considered as acceptable assessment and, moreover, as adequate point of departure for further modeling and calculation. Furthermore, it is evident that verification activities—also on basis of academically reduced experiments—can be performed which in turn will strengthen the sustainability of the approach. In addition, relevant sensitivities can be derived from this assessment, which will provide a feedback to the experiments and their potential layout.

Acknowledgments

The support of the Russian Science Foundation for development of the theoretical background for calculation of the electrical conductivity of the thermal dusty plasma (Grant No. 14-50-00124, D I Zh) and of the Russian Foundation for Basic Research for the experimental investigation of the thermal plasma and development of the diagnostic technique (Grant No. 14-02-90052, O F P) are gratefully acknowledged.

References

[1] Spitzer L 1941 *Astrophys. J.* **93** 369
[2] Goertz C K 1989 *Rev. Geophys.* **27** 271
[3] Mendis D A 2002 *Plasma Sources Sci. Technol.* **11** A219

[4] Shukla P K 2001 *Phys. Plasmas* **8** 1791
[5] Mather T A and Harrison R G 2006 *Surv. Geophys.* **27** 387
[6] Boufendi L and Bouchoule A 1994 *Plasma Sources Sci. Technol.* **3** 262
[7] Winter J and Gebauer G 1999 *J. Nucl. Mater.* **266–9** 228
[8] Bouchoule A 1999 *Dusty Plasmas Physics Chemistry and Technologcial Impacts in Plasma Processing* (New York: Wiley)
[9] Morfill G and Kersten H 2003 *New J. Phys.* **5**
[10] Kersten H, Deutsch H and Kroesen G M W 2004 *Int. J. Mass Spectrom.* **233** 51 special issue: in honour of Tilmann Mark
[11] Matthews L S, Shotorban B and Hyde T W 2013 *Astrophys. J.* **776** 103
[12] Matthews L S, Land V and Hyde T W 2012 *Astrophys. J.* **744** 8
[13] Matthews L S and Hyde T W 2007 Charging of fractal dust agglomerates in a plasma environment *16th IEEE Int. Pulsed Power Conf. (7–22 June 2007)* vol 2, p 1577
[14] Northrop T G 1992 *Phys. Scr.* **45** 475
[15] Kimura H and Mann I 1998 *Astrophys. J.* **499** 454
[16] Ma Q, Matthews L S, Land V and Hyde T W 2013 *Astrophys. J.* **763** 77
[17] Mendis D A, Rosenberg M and Chow V W 1998 *Physics of Dusty Plasmas* ed M Horanyi, S Robertson and B Walch (New York: AIP) p 1
[18] Rosenberg M, Mendis D A and Sheehan D P 1999 *IEEE Trans. Plasma Sci.* **27** 239
[19] Fortov V E, Nefedov A P, Nikitsky V P, Ivanov A I and Lipaev A M 2000 Experimental studies of UV-induced dusty plasmas under microgravity *Frontiers in Dusty Plasmas* ed Y N Y K Shukla (Amsterdam: Elsevier) p 535
[20] Rosenberg M, Mendis D A and Sheehan D P 1996 *IEEE Trans. Plasma Sci.* **24** 1422
[21] Shuler K E and Weber J 1954 *J. Chem. Phys.* **22** 491
[22] Sugden T M and Thrush B A 1951 *Nature* **168** 703
[23] Sodha M S 2014 *Kinetics of Complex Plasmas (Springer Series on Atomic, Optical, and Plasma Physics)* ed G W F Drake (Dordrecht: Springer) vol 81
[24] Bronold F X, Fehske H, Kersten H and Deutsch H 2008 *Phys. Rev. Lett.* **101** 175002
[25] Bronold F X, Fehske H, Kersten H and Deutsch H 2009 *Contrib. Plasma Phys.* **49** 303
[26] Heinisch R L, Bronold F X and Fehske H 2011 *Phys. Rev.* B **83** 195407
[27] Thiessen E, Heinisch R L, Bronolda F X and Fehske H 2014 *Eur. Phys. J. D* **68** 98
[28] Mather T A and Harrison R G 2006 *Surv. Geophys.* **27** 387
[29] Boyle A R and Llewellyn F J 1950 *J. Soc. Chem. Ind.* **69** 173
[30] Nifuku M and Katoh H 2003 *Powder Technol.* **135–136** 234
[31] Mphale K and Heron M 2007 *Tellus B* **59** 766
[32] Mphale K M, Luhanga P V C and Heron M L 2008 *Combust. Flame* **154** 728
[33] Gillman E D and Amatucci W E 2014 *Phys. Plasmas* **21** 060701
[34] Kinefuchi K, Okita K, Funaki I and Abe T 2014 *J. Spacecr. Rockets* **0** 1
[35] Aničin B A, Jojić B, Blagojević D, Adžić M and Milosavljević V 1986 *Combust. Flame* **64** 309
[36] Herdrich G, Laufer R, Gabrielli R A, Dropmann M, Hyde T W and Roeser H-P 2012 *J. Frontiers Aerosp. Eng.* **1** 27
[37] Roth J R 1986 *Introduction to Fusion Energy* (Charlottesville, VA: Ibis)
[38] Einbinder H 1957 *J. Chem. Phys.* **26** 948
[39] Sodha M S and Guha S 1971 *Adv. Plasma Phys.* **4** 219
[40] Herdrich G and Petkow D 2008 *J. Plasma Phys.* **74** 391
[41] Fortov V E, Nefedov A P, Petrov O F, Samarian A A and Chernyschev A V 1996 *Phys. Rev.* E **54** R2236
[42] Fortov V E, Nefedov A P, Petrov O F, Samaryan A A and Chernyshev A V 1997 *JETP* **84** 256
[43] Nefedov A P, Petrov O F and Fortov V E 1997 *Sov. Phys.—Uspekhi* **167** 1215
[44] Dropmann M, Herdrich G, Laufer R, Puckert D, Fulge H, Fasoulas S, Schmoke J, Cook M and Hyde T W 2013 *IEEE Trans. Plasma Sci.* **31** 804
[45] Herdrich G, Auweter-Kurtz M, Kurtz H L, Laux T and Winter M 2002 *J. Thermophys. Heat Transfer* **16** 440
[46] Zhukhovitskii D I, Khrapak A G and Yakubov I T 1984 *Teplofiz. Vys. Temp.* **22** 833
[47] Khrapak A G and Yakubov I T 1981 *Electrons in Dense Gases and Plasmas* (Moscow: Nauka)
[48] Lifshitz E M and Pitaevskii L P 1981 *Physical Kinetics* (Oxford: Pergamon)
[49] Zhukhovitskii D I, Khrapak A G and Yakubov I T 1984 Ionization equilibrium in the plasma with a condensed disperse phase *Plasma Chemistry* vol 11 ed B M Smirnov (Moscow: Energoatomizdat) p 130
[50] Gibson E G 1966 *Phys. Fluids* **9** 2389
[51] Hansen J P 1976 *Phys. Rev.* A **8** 3096
[52] Fomenko V S 1981 *Emission Properties of Materials* (Kiev: Naukova Dumka)
[53] Zimin E P, Mihnevich Z G and Popov V A 1966 *Proc. Symp. Electricity from MHD (Salzburg, Vienna)* vol 3, p 97
[54] Beinar K S and Nikonov V P 1965 *Technol. Electron.* **10** 476
[55] Waldie B and Fells I 1967 *Phil. Trans. R. Soc.* A **261** 490
[56] Kondrat'ev A B, Nefedov A P, Petrov O F and Samaryan A A 1994 *Teplofiz. Vys. Temp.* **32** 452
[57] Nefedov A P, Petrov O F and Vaulina O S 1995 *J. Quant. Spectrosc. Radiat. Transfer* **54** 453
[58] Vaulina O S, Samaryan A A, Chernyshov A V, Nefedov A P and Petrov O F 1999 *Plasma Phys. Rep.* **25** 170
[59] Kosov V F, Molotkov V I and Nefedov A P 1991 *Teplofiz. Vys. Temp.* **29** 633
[60] Glushko A (ed) 1985 *Thermodynamic Properties of Individual Substances* (Moscow: Nauka)
[61] Zhukhovitskii D I, Khrapak A G and Yakubov I T 1983 *Teplofiz. Vys. Temp.* **21** 982